

Collision Efficiencies of Ice Crystals at Low–Intermediate Reynolds Numbers Colliding with Supercooled Cloud Droplets: A Numerical Study

PAO K. WANG AND WUSHENG JI

Department of Atmospheric and Oceanic Sciences, University of Wisconsin—Madison, Madison, Wisconsin

(Manuscript received 16 November 1998, in final form 3 May 1999)

ABSTRACT

The efficiencies with which ice crystals at low–intermediate Reynolds numbers collide with supercooled cloud droplets are determined numerically. Three ice crystal habits are considered here: hexagonal ice plates, broad-branch crystals, and columnar ice crystals. Their Reynolds numbers range from 0.1 to slightly beyond 100. The size of cloud droplets range from a few to about 100 μm in radius. The collision efficiencies are determined by solving the equation of motion for a cloud droplet under the influence of the flow field of the falling ice crystal. The flow fields of the falling ice crystals were determined previously by numerically solving the unsteady Navier–Stokes equations. Features of these efficiencies are discussed. The computed efficiencies are compared with those obtained by previous investigators and improvements are indicated. New results fit better with the observed riming droplet sizes and cutoff riming ice crystal sizes.

1. Introduction

The collision of supercooled cloud droplets with and the subsequent freezing of these droplets on ice crystals, known as the riming process, plays a fundamental role in the formation of precipitation-sized hydrometeors in clouds (Pruppacher and Klett 1997; Cotton and Anthes 1989; Johnson et al. 1993). Recent numerical study by Johnson et al. (1994) indicate that more than 70% of the rainwater produced in a midlatitude deep convective storm comes from the melting of graupel and hail. Even in subtropical thunderstorms, the melting of graupel and hail accounts for about 50% of the rainwater production (Lin and Wang 1997). Since graupel and hail themselves are the products of riming process in clouds, it is logical to expect that riming rates have a significant impact on the rain production rates in convective storms.

In addition, riming involves the phase change of water substance from liquid to solid and hence the release of latent heat into the surrounding air. In a cloud region where riming proceeds at a rapid pace, this heating may become significant enough to influence the thermodynamic structure and, ultimately, the dynamic behavior of the storm.

The riming rate hinges on two quantities: the collision efficiency between ice particles and supercooled droplets, and the coalescence efficiency of the colliding pair.

The coalescence efficiency is usually assumed to be one (i.e., 100%) since observations indicate that at temperatures lower than 0°C a supercooled droplet instantly turns into ice upon collision with an ice surface. The collision efficiency, on the other hand, is a complicated function of ice particle size, shape, density, velocity, and the droplet size. This paper addresses the determination of collision efficiencies. Here we shall restrict our discussion to the collision between pristine ice crystals and supercooled droplets. The riming of graupel and hail where the collectors are usually larger than pristine ice crystals will not be considered here.

In order to determine the collision efficiency between an ice crystal and a water droplet accurately, one either conducts experimental measurements under a controlled laboratory condition or performs calculations based on rigorous theoretical models. The former is a difficult and often expensive task, and thus far only a few measurements were done over limited ranges of ice particle size (Sasyo 1971; Sasyo and Tokue 1973; Kajikawa 1974). On the other hand, theoretical calculations can be relatively economic to perform compared with experimental measurements if properly done. The main obstacles are the accurate formulation and computing algorithm, and the adequacy of computer resources; both can be overcome with reasonable efforts. The present study is based on theoretical calculations.

Theoretical calculations of collision efficiencies between ice crystals and cloud droplets have been performed previously by some investigators. Ono (1969) and Wilkins and Auer (1970) calculated the collision efficiencies between ice disks and droplets based on

Corresponding author address: Dr. Pao K. Wang, Department of Atmospheric and Oceanic Sciences, University of Wisconsin—Madison, 1225 W. Dayton Street, Madison, WI 53706.
E-mail: pao@windy.meteor.wisc.edu

inviscid flow fields past disks. Pitter and Pruppacher (1974) and Martin et al. (1981) performed calculations of the collision efficiency between ice plates and supercooled droplets assuming that the flow fields past hexagonal plates can be approximated by that past thin oblate spheroids. Schlamp et al. (1975) calculated the efficiencies with which columnar ice crystals collide with supercooled droplets assuming that the flow fields past an ice column can be approximated by that past an infinitely long cylinder. While these studies contributed significantly to our early understanding of the onset of riming process, there is room for improvement. Furthermore, all of these studies assumed that flow fields are steady, which is not valid for larger ice crystals that fall in an unsteady attitude (Pruppacher and Klett 1997).

Recently, Ji and Wang (1989, 1991) and Wang and Ji (1997) performed calculations of the flow fields past three different shapes of ice crystals: hexagonal ice plates, broad-branch crystals, and ice columns. The shapes of ice crystals used in their calculations are more realistic than those mentioned before. Also, unsteady features such as eddy shedding were included in the calculations. These improvements ultimately led to more accurate computation of flow fields. The present study is based on the flow fields as determined by Wang and Ji (1997). Using these fields we calculated the collision efficiencies with which ice crystals of the above three shapes collided with supercooled droplets. The details of the formulations, results, and conclusions are reported below.

2. Physics and mathematics

The theoretical problem of determining the collision efficiency between an ice crystal and a supercooled cloud droplet mainly involves the solution of the equation of motion of the droplet in the vicinity of the falling ice crystal. Since the motions occur in a viscous medium, air, the effect of flow fields must be considered. The flow fields around falling ice crystals are complicated and are normally obtained by solving relevant Navier–Stokes equations governing the flow. The information of these flow fields is fed into the equation of motion and the latter is solved (usually by numerical techniques) to determine the “critical trajectory,” that is, the trajectory of the droplet that makes grazing collision with the crystal [see, e.g., chapter 14 of Pruppacher and Klett (1997) for an explanation of the grazing trajectory]. Finally, the collision efficiency is calculated based on the knowledge of the grazing trajectory. In the following, these steps are described one by one.

a. Flow fields around falling ice crystals

As indicated above, the first step of determining the collision efficiency is to determine the flow fields around falling ice crystals. This is done by solving the incom-

pressible Navier–Stokes equations for flow past ice crystals:

$$\frac{\partial \mathbf{u}}{\partial t} + (\mathbf{u} \cdot \nabla) \mathbf{u} = -\frac{\nabla P}{\rho} + \nu \nabla^2 \mathbf{u}, \quad (1)$$

where \mathbf{u} is local flow velocity vector, P the dynamic pressure associated with the flow field, ρ air density and ν the kinematic viscosity of air. In the context of numerical calculations, this equation is often nondimensionalized by utilizing the following nondimensional variables:

$$\begin{aligned} x' &= \frac{x}{a_1}, & \mathbf{u}' &= \frac{\mathbf{u}}{u_\infty}, & t' &= \frac{tu_\infty}{a_1}, \\ P' &= \frac{P}{\rho u_\infty^2}, & \text{Re} &= \frac{2u_\infty a_1}{\nu}, \end{aligned} \quad (2)$$

where x (or y , z) is one of three Cartesian coordinates; a_1 the characteristic dimension of the ice particle; u_∞ the free-stream velocity, which is equal to the terminal fall velocity of the ice crystal; and Re is the Reynolds number relevant to the flow. All primed quantities are nondimensional. Using these dimensionless variables, we can write the nondimensional Navier–Stokes equation and the continuity equation as (after dropping the primes)

$$\frac{\partial \mathbf{u}}{\partial t} + \mathbf{u} \cdot \nabla \mathbf{u} = -\nabla P + \frac{2}{\text{Re}} \nabla^2 \mathbf{u} \quad (3)$$

$$\nabla \cdot \mathbf{u} = 0. \quad (4)$$

The ideal boundary conditions appropriate for the present problems are

$$\mathbf{u} = 0 \quad \text{at the surface of the ice crystal, and} \quad (5)$$

$$\mathbf{u} = 1 \cdot \mathbf{e}_z \quad \text{at infinity,} \quad (6)$$

where \mathbf{e}_z is a unit vector in the free stream direction. The details of the numerical procedure have been given in a recent paper by Wang and Ji (1997), so they will not be repeated here. The velocity vectors so obtained are input into the equation of motion to be described below.

b. Equation of motion and droplet trajectory

The equation of motion of a cloud droplet of radius a_2 in the vicinity of a falling ice crystal of characteristic dimension a_1 is

$$m \frac{d\mathbf{V}}{dt} = m \frac{d^2 \mathbf{r}}{dt^2} = \mathbf{F}_g + \mathbf{F}_D, \quad (7)$$

where m is the mass of the droplet, \mathbf{V} its velocity, \mathbf{r} its position vector, \mathbf{F}_g the buoyancy-adjusted gravitational force, and \mathbf{F}_D the hydrodynamic drag force due to the flow. These two forces are expressed as

$$\mathbf{F}_g = mg \left(\frac{\rho_w - \rho_a}{\rho_w} \right), \quad (8)$$

where ρ_w and ρ_a are the density of water and air, respectively, and

$$\mathbf{F}_D = 6\pi\eta a_2 \left(\frac{C_D \text{Re}}{24} \right) (\mathbf{V} - \mathbf{u}). \quad (9)$$

In order to calculate the drag force (9), we need to input the local flow velocity \mathbf{u} at each time step. That value comes from the solution of (3).

In order to solve Eq. (7), it is also necessary to specify an initial condition. The appropriate initial condition here is the initial horizontal offset y of the droplet from the vertical line passing through the center of the falling ice crystal (see Pruppacher and Klett 1997, p. 569). Needless to say, this offset has to be set at a distance sufficiently upstream to ensure that the droplet is progressing in a straight line at the time. In this study the initial offset was set at 20 radii upstream of the ice crystal and it was proven adequate for the above-stated purpose. With this initial condition in place, Eq. (7) can be solved for \mathbf{V} and hence \mathbf{r} of the droplet as a function of time. The latter defines its trajectory.

To determine the collision efficiency, we need to determine the critical initial offset y_c of the droplet such that it will make a grazing collision with the ice crystal. An initial offset greater than y_c would result in a miss, whereas one smaller than y_c would result in a hit. In the present study, a bisection technique, similar to that used in Miller and Wang (1989), was used to determine y_c . Once this is done, the next step is determining the collision efficiency E .

c. Collision efficiency

Since the collector is an ice crystal that is usually not a sphere, it is important to take a closer examination of the proper definition of collection efficiency here. The old definition of collision efficiency based on spherical symmetry [e.g., Pruppacher and Klett 1997, Eq. (14-1)] is inappropriate here. The proper definition of E here is the one given by Wang (1983), namely,

$$E = \frac{K}{K^*} = \frac{A}{A^*}, \quad (10)$$

where K is the collision kernel, K^* the geometrical collision kernel, A the collision cross section, and A^* the geometrical collision cross section (see Fig. 1 for a clearer definition). The relation between the collision kernel and collision cross section is

$$K = A(\mathbf{V} - \mathbf{u}). \quad (11)$$

This definition takes care of the nonspherical shape of the ice crystal and is more general than the usual definition of collision efficiency based on the "radius" of the collector that is strictly valid for only spheres. Thus

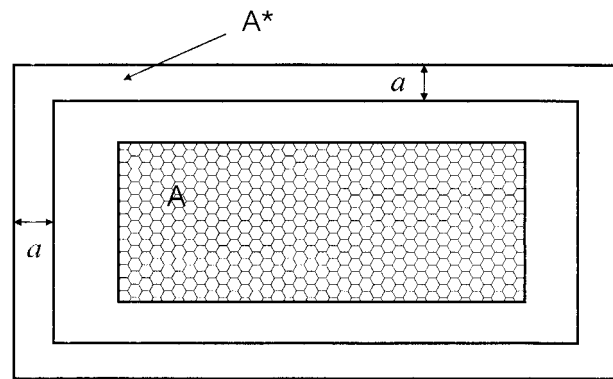


FIG. 1. A schematic explanation of the collision cross section, using a columnar ice crystal as an example. The hexagon-filled area represents the collision cross section A , the middle rectangle the cross section (horizontal projection) of the ice column. The outermost rectangle represents the geometrical collision cross section A^* .

cloud droplets located within A (or K) will be eventually collected by the ice crystal and turn into rime. Note that the definition of collision efficiency as given by (10) assumes that the droplets are of the same size. The efficiency would vary if we deal with a distribution of drop sizes, but this is not what we treat here.

In the case of unsteady flow fields, the trajectory of a droplet starting from a certain initial offset was determined by averaging a few trajectories over a cycle of eddy shedding periods. This was done for a few cases, but it was later found to be unnecessary because these trajectories vary very little as grazing collisions in this study all occur in the upstream regions where flow fields are steady. In addition, droplets are massive enough to defy small fluctuations in the flow fields. This may not be the case if the collection of submicron particles by hydrometeors is considered since rear capture may occur in that case (e.g., Wang et al. 1978; Wang and Jaroszyk 1991) and the unsteady fields in the downstream would have greater effect.

3. Results and discussion

Ice crystal collectors of three different habits are considered in this study: columnar ice crystals (approximated as finite circular cylinders), hexagonal ice plates, and broad-branch ice crystals. Tables 1, 2, and 3 show the dimensions of these ice crystals. These are the same set of ice crystals whose flow fields and ventilation coefficients were computed by Wang and Ji (1997) Ji and Wang (1999), respectively. Figure 2 shows several trajectories of a droplet of $2\text{-}\mu\text{m}$ radius moving around a falling broad-branch crystal of $\text{Re} = 10$. Of the eight trajectories shown here, trajectories 1, 2, 6, 7, and 8 are misses, whereas trajectories 3, 4, and 5 are hits. Trajectory 4 is the central trajectory, while 3 and 5 are grazing trajectories.

Note that since the collector ice crystals are not spheres, the critical initial offset y_c does not possess

TABLE 1. Reynolds numbers, dimensions, and capacitance of columnar ice crystals in the present study. The quantities are dimensionless.

N_{Re}	Radius (μm)	Length (μm)	Capacitance
0.2	23.5	67.1	1.3628
0.5	32.7	93.3	1.3628
0.7	36.6	112.6	1.4054
1.0	41.5	138.3	1.4535
2.0	53.4	237.4	1.6511
5.0	77.2	514.9	2.0151
10.0	106.7	1067	2.5067
20.0	146.4	2440	3.3959

circular symmetry but rather is a function of the azimuthal angle. The asymmetry is most easily shown by the shape of the collision cross section A formed by connecting y_c 's of all angles. Figures 3, 4, and 5 show examples of these collision cross sections for droplets of various sizes colliding with the three types of ice crystals. It is immediately clear that the shapes of the A 's are more or less similar to the ice crystal cross sections themselves. When droplets are small, their collision cross sections (and hence the collision efficiencies) are usually (but not always) smaller. As the droplets become larger, the collision cross sections become larger and the shapes are closer to the cross sections of the ice crystals. This behavior is obviously because of the inertia of the droplet relative the strength of the hydrodynamic drag force, a reasoning that has been discussed in great detail by Pruppacher and Klett (1997). When droplets are small, their inertias are small compared to the drag and their trajectories are close to the streamlines of the flow fields, which are generally curved around the crystal. Thus the shape of the collision cross section would be different from the crystal. When droplets are larger, their inertia becomes greater and their trajectories are straighter; hence, the collision cross sections have shapes closer to that of the crystal.

a. Hexagonal plates

Figures 6, 7, and 8 show the computed collision efficiencies for the three crystal habits. The case of hexagonal ice plates is shown in Fig. 6. The general feature here is that, at a fixed crystal Reynolds number, the

TABLE 2. Reynolds numbers, dimensions, and capacitance of hexagonal ice plates in the present study. The quantities are dimensionless.

N_{Re}	Radius (μm)	Thickness (μm)	Capacitance
1.0	80.0	18.0	0.7298
2.0	113.3	20.0	0.6977
10.0	253.3	32.0	0.6639
20.0	358.2	37.0	0.6485
35.0	473.8	41.0	0.6371
60.0	620.0	45.0	0.6278
90.0	750.0	48.0	0.6221
120.0	850.0	49.0	0.6179

TABLE 3. Reynolds numbers and dimensions of broad-branch ice crystals in the present study.

N_{Re}	Radius (μm)	Thickness (μm)
1.0	100.0	15.0
2.0	125.0	18.0
10.0	350.0	32.0
20.0	500.0	40.0
35.0	750.0	50.0
60.0	1000.0	60.0
90.0	1250.0	65.0
120.0	1550.0	73.0

efficiency is very small when the droplet is small due to its small inertia, as explained previously. In the cases of $Re = 1.0$ and 2.0 , the efficiency drops to very small value ($<10^{-4}$) for droplets with radii less than $9 \mu\text{m}$. For higher- Re (larger ice crystals) cases, this efficiency drop is more gradual and there is no sharp cutoff. This is in contrast with earlier studies where a cutoff at $a_2 \approx 5 \mu\text{m}$ occurs (e.g., Pitter and Pruppacher 1974; Pitter 1977). Instead, the efficiency remains finite even for droplets as small as $2.5 \mu\text{m}$, which is in good agreement with Kajikawa's (1974) experimental results. Recent observational studies also confirm that many frozen droplets on the rimed ice crystals are smaller than $5 \mu\text{m}$. The reason that some previous field observations indicated the scarcity of frozen droplets with a radius less than $5 \mu\text{m}$ on planar ice crystals (e.g., Harimaya 1975; Wilkins and Auer 1970; Kikuchi and Ueda 1979; and D'Enrico and Auer 1978) is probably due to the local

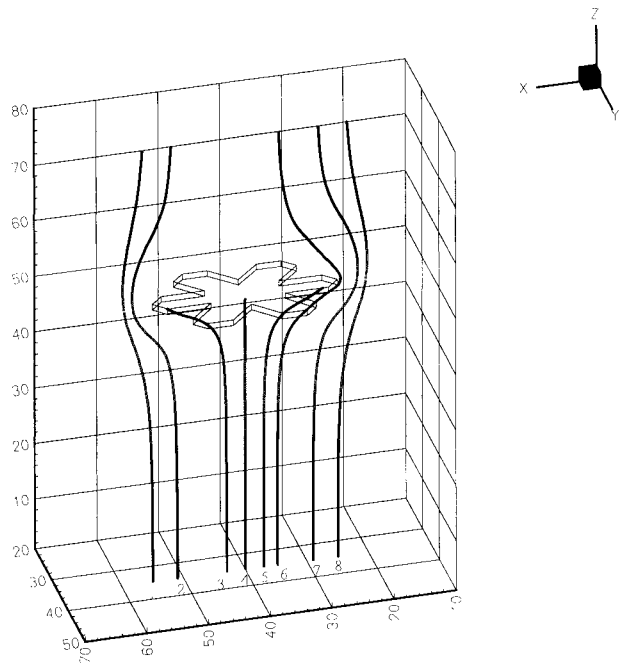


FIG. 2. Trajectories of a droplet of $2 \mu\text{m}$ in radius moving in the vicinity of a falling broad-branch ice crystal at $Re = 10$. Trajectories 1, 2, 6, 7, and 8 are misses, and trajectories 3, 4, 5 are hits.

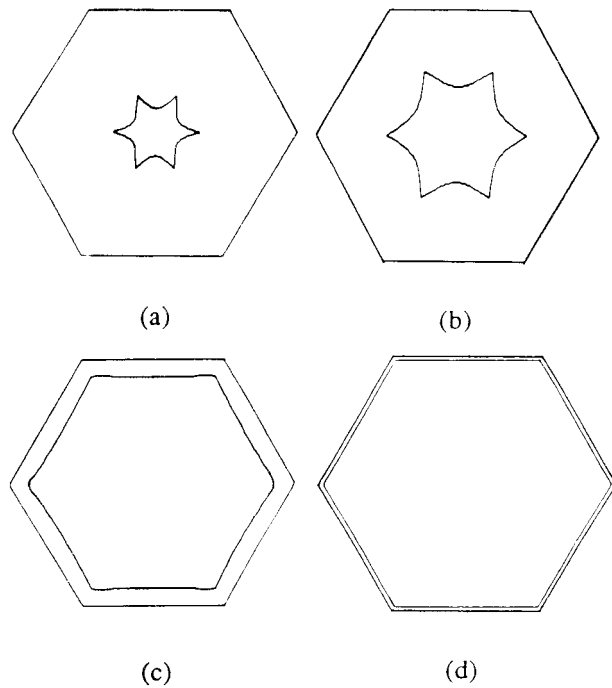


FIG. 3. Shape of collision cross sections for a hexagonal ice plate at $Re = 20$, colliding with supercooled droplets of radius r . The fixed hexagon is the cross section of the ice plate: (a) $r = 3 \mu\text{m}$, (b) $r = 5 \mu\text{m}$, (c) $r = 11 \mu\text{m}$, and (d) $r = 27 \mu\text{m}$.

microstructure of clouds instead of intrinsic collision mechanism (Pruppacher and Klett 1997).

As the drop size increases, the efficiency increases rapidly. The efficiency reaches a peak or a plateau, depending on the Reynolds number of the ice crystal, and then drops off sharply for further increasing drop size. The drop off of efficiency is apparently due to the increasing terminal velocity of the droplet. When the collector ice crystal and the droplet have about the same velocity, collision is nearly impossible and the efficiency becomes very small (Pitter and Pruppacher 1974; Pitter 1977; Martin et al. 1981; Pruppacher and Klett 1997). The efficiency maxima take the shape of peaks in smaller- Re cases but become broader plateaus as the ice crystal Re increases, apparently because the larger crystals can collide with droplets of broader size range and maintain fairly high efficiencies. Due to their sizes, smaller crystals are quickly “outrun” by droplets as droplets become larger and hence are unable to perform the collision.

b. Broad-branch crystals

Figure 7 shows the collision efficiency for broad-branch crystals colliding with supercooled droplets. The main features are similar to those for hexagonal plates. The collision efficiency for $Re = 1.0$ is practically zero, representing an inability to rime. This cutoff of riming ability will be discussed further below.

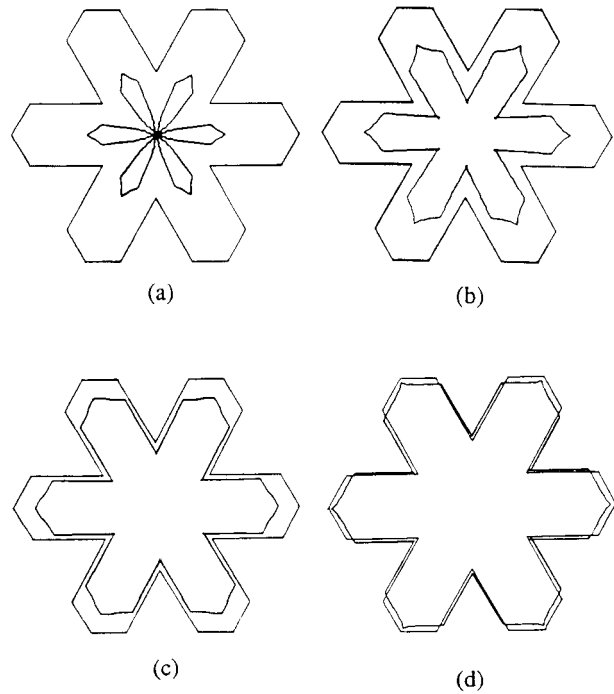


FIG. 4. Same as Fig. 3 except for a broad-branch crystal at $Re = 35$: (a) $r = 5 \mu\text{m}$, (b) $r = 9 \mu\text{m}$, (c) $r = 15 \mu\text{m}$, and (d) $r = 36 \mu\text{m}$.

The collision efficiencies of broad-branch crystals are in general smaller than those of hexagonal plates at the same Reynolds number. The maximum efficiencies in the plateau region are about 0.9, unlike the case of hexagonal plates, whose maximum efficiencies are near 1.0. This is probably due to the more open structure of a broad-branch crystal that would allow the droplet to “slip through” the gap between branches. The width of the “plateau” is also much narrower than the corre-

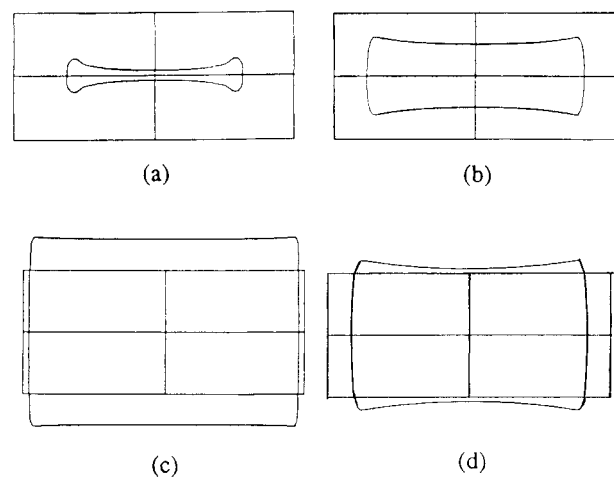


FIG. 5. Same as Fig. 3 except for a columnar ice crystal at $Re = 2.0$: (a) $r = 4 \mu\text{m}$, (b) $r = 6 \mu\text{m}$, (c) $r = 35 \mu\text{m}$, and (d) $r = 43 \mu\text{m}$.

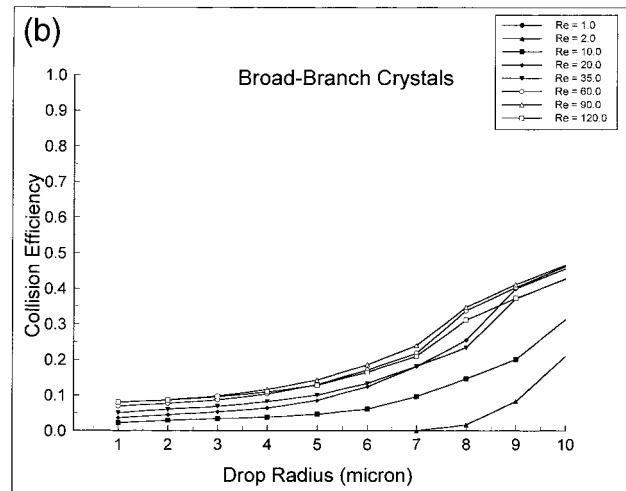
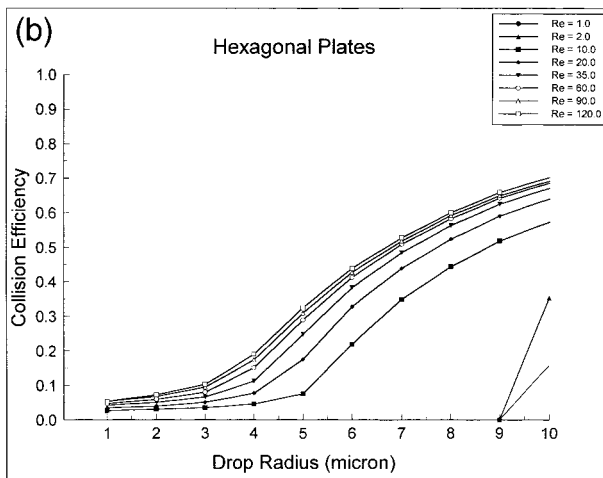
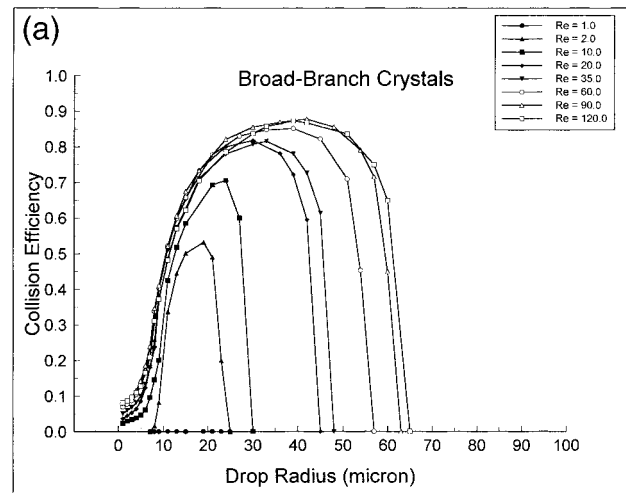
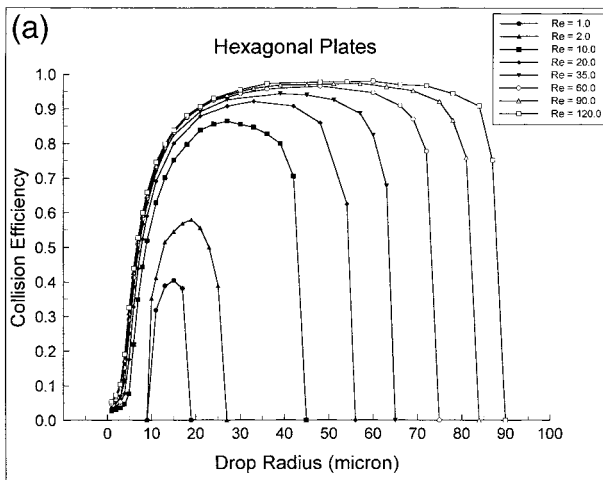


FIG. 6. (a) Collision efficiencies of hexagonal ice plates colliding with supercooled droplets determined in the present study. The last data points (at large drop size end) for $Re = 20$ to 120 are extrapolated. (b) The same as (a) except the abscissa is limited for drop size up to $10 \mu\text{m}$.

FIG. 7. (a) Collision efficiencies of broad-branch crystals colliding with supercooled droplets determined in the present study. The last data points (at large drop size end) for $Re = 20$ to 120 are extrapolated. (b) The same as (a) except the abscissa is limited for drop size up to $10 \mu\text{m}$.

sponding case of hexagonal plate. This is most likely due to the smaller fall velocity of the broad-branch crystal (as compared to a hexagonal plate at the same Reynolds number) and hence is outrun by a droplet sooner.

If the above reasoning holds true, then it implies that stellar crystals, which have even more open structure, probably have collision efficiencies similar to or smaller than those of broad-branch crystals. However, the same cannot be said for the case of dendrites since they have more intricate small branches that may afford them to capture droplets with higher efficiency.

c. Columnar ice crystals

Collision efficiencies of columnar ice crystals colliding with supercooled droplets are shown in Fig. 8. The general features here look very similar to those in Fig.

6 despite the difference in Reynolds number ranges in these two cases. This is because the difference in Re is a superficial one since the Reynolds numbers of the falling columns are determined based on their radii instead of lengths. Had the latter been used, the two sets of Re 's would be much closer in magnitude.

The plateaus in Fig. 8 are not as flat as those in Fig. 6 but exhibit a downhill slope toward larger drop size. Although the exact cause is not known, this is likely due to the higher asymmetry of a column than a plate. The effect of this asymmetry would become more pronounced as the drop size increases.

d. Finite versus infinite cylinders

It is educational to examine the differences between the collection efficiency results of finite and infinite cyl-

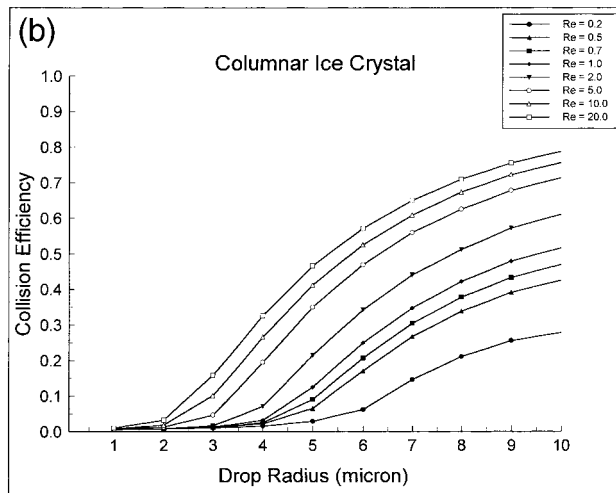
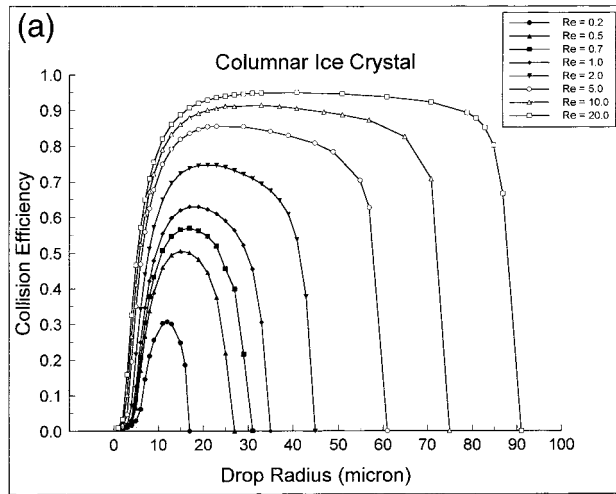


FIG. 8. (a) Collision efficiencies of columnar ice crystals colliding with supercooled droplets determined in the present study. (b) The same as (a) except the abscissa is limited for drop size up to 10 μm .

inder approximations of columnar ice crystals so that we can assess the validity of the infinite cylinder approach that was used by several studies before (e.g., Schlamp et al. 1975). Figure 9 shows two sets of collection efficiency curves, one for finite and the other for infinite cylinders, for $Re = 0.5, 1.0, 5.0,$ and 20.0 . For the cases of $Re = 0.5$ and 1.0 , we see that the finite cylinders have higher efficiencies than the infinite ones. The difference is greater for $Re = 0.5$ and becomes smaller for $Re = 0.1$. For the cases of $Re = 5.0$ and 20.0 , the two sets of collection efficiencies are almost on top of each other for drop sizes smaller than $30 \mu\text{m}$. The differences become more pronounced for larger drops. The enhanced efficiencies of the infinite cylinders may be due to the artificial effect of the superposition technique used by Schlamp et al. (1975) and hence probably do not reflect the real effect of the infinite length assumption.

The above paragraph states that the discrepancies be-

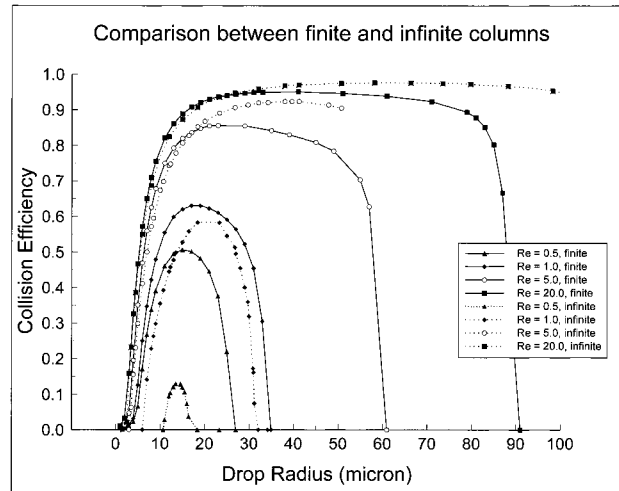


FIG. 9. Comparison between the collision efficiencies for finite cylinders (present results) and infinite cylinders (Schlamp et al. 1975) for $Re = 0.5, 1.0, 5,$ and 20 .

tween the two sets of curves are more important when the columns are small and become less significant when column size (and hence Reynolds number) increases. This is to be anticipated because, in the present study, smaller columns have aspect ratios that are much different from infinite long cylinders; therefore, the collision efficiencies would also show greater differences. For larger columns, the aspect ratios are closer to those of infinite cylinders and hence the collision efficiencies are also closer to the latter.

In short, using infinite cylinder approximation in treating the collision between columnar ice crystals and supercooled drops is valid when the drop size is between a few micrometers and about $30 \mu\text{m}$, and when the ice column Reynolds number is greater than 5. Since the flow field around an infinitely long cylinder is easier to compute than that of finite cylinders, this approximation may be useful when computing resource is of concern.

When the drop size becomes smaller than a few micrometers, the infinite cylinder model underpredicts the collision efficiencies for the same reason discussed in section 3a regarding hexagonal plate results.

e. Riming cutoff

Earlier observational studies indicated that there seems to exist a cutoff size of ice crystals below which riming cannot occur (Ono 1969; Wilkins and Auer 1970; Harimaya 1975). Since riming is due to the collision between ice crystals and supercooled droplets, the cutoff would occur at a crystal size where the collision efficiency is zero. Earlier theoretical studies of Pitter and Pruppacher (1974) and Pitter (1977) put the riming cutoff size of planar ice crystals at $300 \mu\text{m}$, which seemed to agree with observations at the time. However, recent studies indicate riming cutoff sizes smaller than this

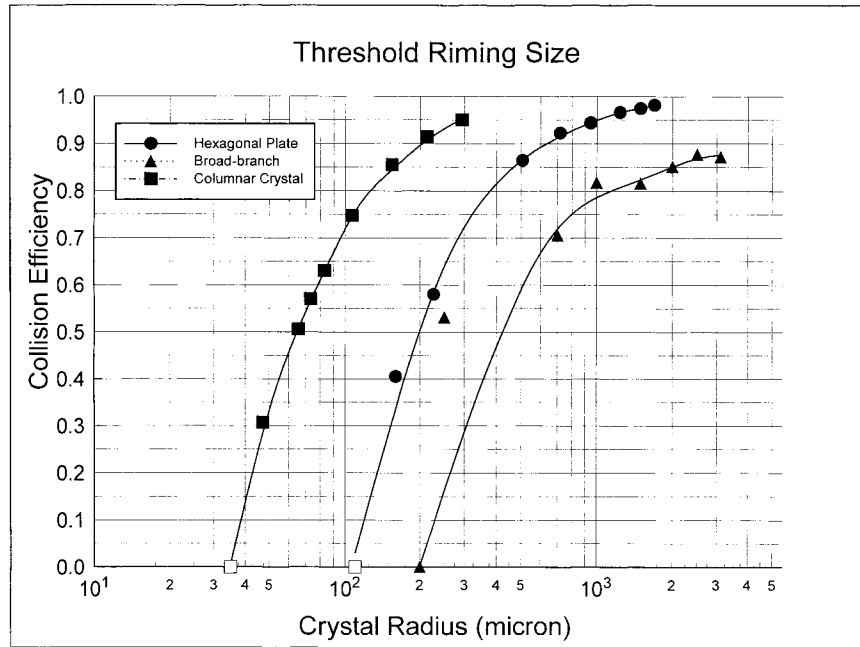


Fig. 10. Cut off riming ice crystal sizes as extrapolated by the present results. For broad-branch crystals, the data point for crystal radius 2.5 μm was ignored when obtaining the best fit.

value (Devulapalli and Collett 1994; Collett and Xu 1999, personal communication). Results of collision efficiencies computed in the present study can be used to predict the cutoff riming crystal size. This is done by plotting the maximum collision efficiency (the peak point of each curve in Figs. 6–8) as a function of crystal size for each crystal habit, as shown in Fig. 10. The point where the extrapolated curve intersects with the x axis (where $E = 0$) indicates the cutoff size of ice crystal below which riming would not occur. Using this method, we determine that the riming cutoff size is 35 μm for columnar ice crystals, 110 μm for hexagonal plates, and 200 μm for broad-branch crystals. These values are close to the observations of Wilkins and Auer (1970), Reinking (1979), and Bruntjes et al. (1987), as summarized in Table 4.

4. Conclusions and outlooks

The collision efficiencies of three types of ice crystals colliding with supercooled water drops are computed

and presented above. The main improvements in the present study over previous studies are as follows.

- 1) More realistic ice crystal shapes are adopted, especially the finite length of the columns and the broad-branch crystals whose efficiencies have never reported before.
- 2) More accurate flow fields, including the 3D and unsteady features, are used to determine the grazing trajectories.

The improvements have been demonstrated by the more accurate prediction of the captured droplet sizes and the cutoff riming crystal sizes. We believe the improved collision efficiency values will lead to more accurate growth-rate calculations of ice particles in clouds.

The results presented in this paper pertain to relatively small and pristine ice crystals colliding with small supercooled droplets, so they are mainly applicable to initial stages of riming process when ice particles have not grown too much. When riming has been going on for a longer time, the ice crystal gradually loses its pristine

TABLE 4. Observed critical riming size. The code after the crystal habit is the Magono and Lee (1966) classification of natural snow crystals.

Crystal habit	Wilkins and Auer (1970)	Reinking (1979)	Bruntjes et al. (1987)
Hexagonal plate (Pla)	—	—	$d = 150 \mu\text{m}$
Broad-branch crystal (Plc)	—	$d = 275 \mu\text{m}$	$d = 240 \mu\text{m}$
Columnar crystal (Cle)	$l = 100 \mu\text{m}, d = 40 \mu\text{m}$	—	$l = 125 \mu\text{m}, d = 40 \mu\text{m}$
Long solid column (Nle)	$l = 100 \mu\text{m}, d = 30 \mu\text{m}$	—	—

shape. However, as long as the basic shape of the ice crystal in question is still discernable, we believe the present results are still useful for estimating the riming efficiency as the flow fields would not differ too much. As riming goes further, eventually the original shape of the ice crystal becomes unrecognizable. The pristine ice assumption no longer applies at this stage.

As indicated before, the coalescence of the supercooled drop with the ice surface is assumed to be 100%, so that the case where droplets may bounce off from the ice surface is not considered. It is a much more complicated task to determine theoretically the riming rates of larger ice particles such as graupel and hail, where particles are relatively large and may fall in a zigzag attitude.

Acknowledgments. This work is partially supported by NSF Grants ATM-9314465, ATM-9633424, ATM-9714158, and ATM-9907761 to the University of Wisconsin—Madison. PKW would like to thank Alexander von Humboldt, Foundation of Germany, for the Senior Research Humboldt Award he received, and Johnson Wax Company of Racine, Wisconsin, for a distinguished fellowship to his research group that also contributed to this work.

REFERENCES

- Bruntjes, R. T., A. J. Heymsfield, and T. W. Krauss, 1987: An examination of double-plate ice crystals and the initiation of precipitation in continental cumulus clouds. *J. Atmos. Sci.*, **44**, 1331–1349.
- Cotton, W. R., and R. A. Anthes, 1989: *Storm and Cloud Dynamics*. Academic Press, 880 pp.
- D'Enrico, R. E., and A. H. Auer, 1978: An observational study of the accretional properties of ice crystals of simple geometric shapes. Preprints, *Conf. on Cloud Physics and Atmospheric Electricity*, Issaquah, WA, Amer. Meteor. Soc., 114–121.
- Devulapalli, S. S. N., and J. L. Collett Jr., 1994: The influence of riming and frontal dynamics on winter precipitation chemistry in level terrain. *Atmos. Res.*, **32**, 203–213.
- Harimaya, T., 1975: The timing properties of snow crystals. *J. Meteor. Soc. Japan.*, **53**, 384–392.
- Ji, W., and P. K. Wang, 1989: Numerical simulation of three-dimensional unsteady viscous flow past hexagonal ice crystals in the air—Preliminary results. *Atmos. Res.*, **25**, 539–557.
- , and —, 1991: Numerical simulation of three-dimensional unsteady viscous flow past finite cylinders in an unbounded fluid at low intermediate Reynolds numbers. *Theor. Comput. Fluid Dyn.*, **3**, 43–59.
- , and —, 1999: Ventilation coefficients for falling ice crystals in the atmosphere at low–intermediate Reynolds numbers. *J. Atmos. Sci.*, **56**, 829–836.
- Johnson, D. E., P. K. Wang, and J. M. Straka, 1993: Numerical simulation of the 2 August 1981 CCOPE supercell storm with and without ice microphysics. *J. Appl. Meteor.*, **32**, 745–759.
- , —, and —, 1994: A study of microphysical processes in the 2 August 1981 CCOPE supercell storm. *Atmos. Res.*, **33**, 93–123.
- Kajikawa, M., 1974: On the collection efficiency of snow crystals for cloud droplets. *J. Meteor. Soc. Japan*, **52**, 328–336.
- Kikuchi, K., and H. Uyeda, 1979: Cloud droplets and rain drops collected and frozen on natural snow crystals. *J. Meteor. Soc. Japan*, **57**, 273–281.
- Lin, H.-M., and P. K. Wang, 1997: A numerical study of microphysical processes in the 21 June 1991 northern Taiwan mesoscale precipitation system. *Terr. Atmos. Oceanic Sci.*, **8**, 385–404.
- Martin, J. J., P. K. Wang, H. R. Pruppacher, and R. L. Pitter, 1981: A numerical study of the effect of electric charges on the efficiency with which planar ice crystals collect supercooled water drops. *J. Atmos. Sci.*, **38**, 2462–2469.
- Miller, N. L., and P. K. Wang, 1989: A theoretical determination of the efficiency with which aerosol particles are collected by falling columnar ice crystals. *J. Atmos. Sci.*, **46**, 1656–1663.
- Ono, A., 1969: The shape and riming properties of ice crystals in natural clouds. *J. Atmos. Sci.*, **26**, 138–147.
- Pitter, R. L., 1977: A reexamination of riming on thin ice plates. *J. Atmos. Sci.*, **34**, 684–685.
- , and H. R. Pruppacher, 1974: A numerical investigation of collision efficiencies of simple ice plates colliding with supercooled drops. *J. Atmos. Sci.*, **31**, 551–559.
- Pruppacher, H. R., and J. D. Klett, 1997: *Microphysics of Clouds and Precipitation*. 2d ed. Kluwer Academic, 954 pp.
- Reinking, R., 1979: The onset and steady growth of snow crystals by accretion of droplets. *J. Atmos. Sci.*, **36**, 870–881.
- Sasyo, Y., 1971: Study of the formation of precipitation by the aggregation of snow particles and the accretion of cloud droplets on snowflakes. *Pap. Meteor. Geophys.*, **22**, 69–142.
- , and H. Tokue, 1973: The collection efficiency of simulated snow particles for water droplets (preliminary report). *Pap. Meteor. Geophys.*, **24**, 1–12.
- Schlamp, R. J., H. R. Pruppacher, and A. E. Hamielec, 1975: A numerical investigation of the efficiency with which simple columnar ice crystals collide with supercooled water drops. *J. Atmos. Sci.*, **32**, 2330–2337.
- Wang, P. K., 1983: On the definition of collision efficiency of atmospheric particles. *J. Atmos. Sci.*, **40**, 1051–1052.
- , and T. Jaroszyk, 1991: The grazing collision angle of aerosol particles colliding with infinitely long circular cylinders. *Aerosol Sci. Tech.*, **15**, 149–155.
- , and W. Ji, 1997: Simulation of three-dimensional unsteady flow past ice crystals. *J. Atmos. Sci.*, **54**, 2261–2274.
- , S. N. Grover, and H. R. Pruppacher, 1978: On the effect of electric charges on the scavenging of aerosol particles by cloud and small rain drops. *J. Atmos. Sci.*, **35**, 1735–1743.
- Wilkins, R. D., and A. H. Auer Jr., 1970: Riming properties of hexagonal ice crystals. Preprints, *Conf. on Cloud Physics*, Fort Collins, CO, Amer. Meteor. Soc., 81–82.